
Numerical study of immiscible CO₂ flooding in thick reservoirs with positive rhythm

Shu Wang*

Key Laboratory of Petroleum Resources Research,
Institute of Geology and Geophysics,
Chinese Academy of Sciences,
No. 19, Beitucheng Western Road,
Chaoyang District, Beijing, 100029, China
Email: wangshu@mail.iggcas.ac.cn
Email: wangshu505@163.com
*Corresponding author

Duoxing Yang

China Earthquake Administration,
Institute of Crustal Dynamics,
No. 1, Anningzhuang Rd, Haidian District,
Beijing, 100085, China
Email: dxyangcea@yahoo.com

Xinmin Song, Desheng Ma and Jian Gao

Research Institute of Petroleum Exploration and Development,
PetroChina,
No. 20, Xueyuan Rd, Haidian District,
Beijing, 100083, China
Email: sxm@petrochina.com.cn
Email: mads6@petrochina.com.cn
Email: gaojinacor@petrochina.com.cn

Abstract: Benefiting from the development of carbon capture and storage (CCS) technology, CO₂ flooding for enhanced oil recovery (EOR) has become increasingly attractive to the petroleum industry. This paper presents a numerical study about the feasibility and efficiency of the immiscible CO₂ flooding process, which is a potential tertiary oil recovery method for use after water flooding, with advantages of lower cost and fewer facility requirements than miscible CO₂ flooding. A numerical simulation model established from laboratory experimental results was used to predict fluid behaviour and influence factors of immiscible CO₂ flooding in thick reservoirs with positive rhythm to enhance oil recovery after water flooding. Injection and confining pressure conditions are both important to the displacement process and results.

Keywords: immiscible CO₂ flooding; enhanced oil recovery; EOR; thick reservoir, positive rhythm; numerical simulation; multiphase flow.

Reference to this paper should be made as follows: Wang, S., Yang, D., Song, X., Ma, D. and Gao, J. (2017) 'Numerical study of immiscible CO₂ flooding in thick reservoirs with positive rhythm', *Progress in Computational Fluid Dynamics*, Vol. 17, No. 1, pp.34–41.

Biographical notes: Shu Wang is a postdoctoral fellow in the Institute of Geology and Geophysics, Chinese Academy of Sciences. She holds a PhD in Geology. She focused on CO₂ capture and geological storage and enhanced oil recovery by CO₂ during the doctor degree, and involved in several research projects about CCS. Her recent research interests involve behaviours of multi-phase flow in porous media.

Duoxing Yang is a Full Professor in the Institute of Crustal Dynamics, CEA. His research interests involve heat and mass transfer in porous media. He holds a PhD in Hydrology. He is an editorial board member of *International Journal on Numerical and Analytical Method in Engineering* (IRENA).

Xinmin Song is a Research Professor of Research Institute of Petroleum Exploration and Development (RIPED), PetroChina, conducting oil and gas field development. He holds a PhD in Structural Geology. He is the Vice President of RIPED.

Desheng Ma is a Research Professor of Research Institute of Petroleum Exploration and Development (RIPED), PetroChina, doing researches on enhanced oil recovery. He holds a PhD in Oil-Gas Field Development Engineering. He is the Director of Department of Enhanced Oil Recovery, RIPED.

Jian Gao is a Senior Engineer of Research Institute of Petroleum Exploration and Development (RIPED), PetroChina, doing researches on oil displacement by core analysis and multi-scale reservoir physical simulation. He holds a PhD in Oil-Gas Field Development Engineering.

1 Introduction

Enhanced oil recovery (EOR) technologies are increasingly important to the petroleum industry. After decades of development, water flooding is one of the most successful and extensively used secondary recovery methods (Liu et al., 2012; Romero-Zerón, 2012), which uses injected water to maintain pressure and drive reservoir fluids toward production wells. However, the main oilfields of eastern China contain many thick reservoirs of fluvial facies with positive rhythm, where permeability increases from top to bottom. Under the double effects of heterogeneity and gravitational differentiation, water breakthrough in the lower high-permeability layers rapidly results in low sweep efficiency, poor oil recovery, and high water cut of production (Niu et al., 2006; Wen, 2012). After water flooding, oil recovery is usually about 40% to 50% of the original oil in place (OOIP) (Cao and Gu, 2013; Bikkina et al., 2016).

Many efforts have been made to further improve oil recovery after water flooding in thick reservoirs with positive rhythm, including perfecting well patterns, optimising water injection modes, and using horizontal wells (Gu and Zhai, 2005; Wang et al., 2006; Tan, 2009; Al-Hinai et al., 2010; Cui et al., 2010; Wang et al., 2012; Liu, 2012; Ding et al., 2013; Qu et al., 2014). Although gas flooding has been considered as a potential tertiary oil recovery technique, little research has focused on it in such reservoirs. In recent years, CO₂ flooding for EOR has become increasingly attractive to the petroleum industry, because CO₂, a main greenhouse gas (GHG), is a major contributor to the significantly accelerating rise in average global temperature and, thus, the consequent effects of climate change (Sun et al., 2016). With the development of carbon capture and storage (CCS) technology, CO₂ flooding can not only improve oil recovery, but also considerably reduce GHG contributions to climate change (Wang et al., 2013).

CO₂ flooding can be divided into miscible, immiscible, and near-miscible processes based on different reservoir characteristics and pressure conditions (Cao and Gu, 2012; Song et al., 2013). It is necessary to reach the minimum miscibility pressure (MMP) for miscible CO₂ flooding (Ren et al., 2015). As a result, the cost of miscible CO₂ flooding is much higher. Moreover, in most oilfields of eastern

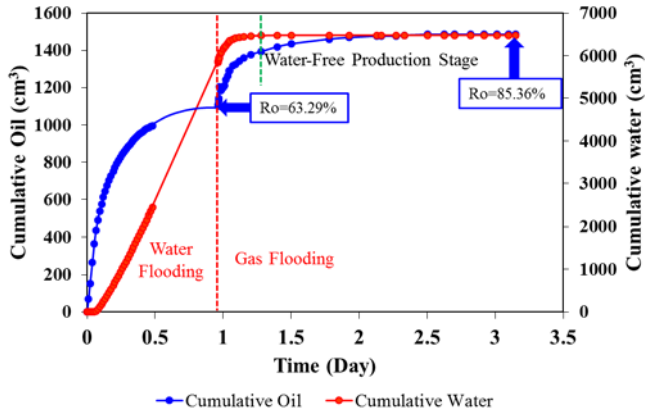
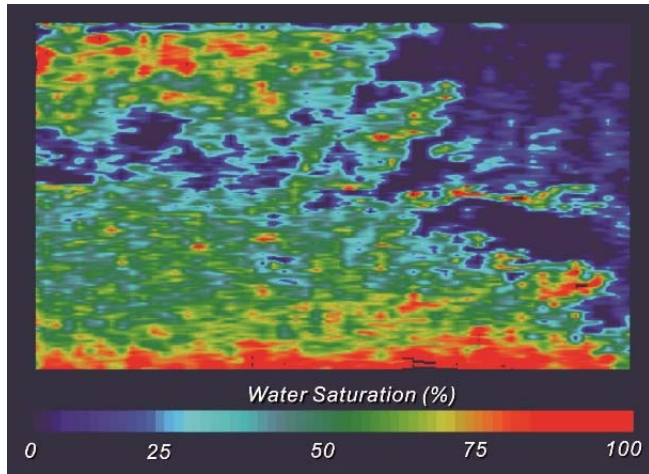
China, miscible CO₂ flooding is difficult because of limitations of reservoir conditions and oil properties (Duan et al., 2016). Therefore, low-cost immiscible CO₂ flooding should be attempted after water flooding.

This paper focuses on the feasibility and efficiency of immiscible CO₂ flooding as an EOR method in thick reservoirs with positive rhythm. A numerical simulation model was established based on a laboratory experiment, the results of which were used to optimise the model. Several predictions were made about the effect of immiscible CO₂ flooding and influencing factors, such as injection and confining pressures. Migration of CO₂ during flooding was also considered in this paper.

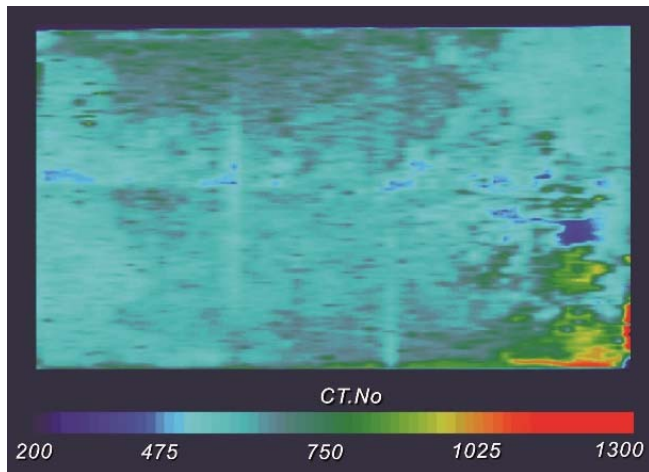
2 Laboratory experiment and results

A laboratory experiment was carried out to establish a database for model building and historical matching of the numerical simulation. The experiment used an artificial consolidated sandstone model to simulate a heterogeneous, thick reservoir. The mould for the model is 50 cm in length, 4 cm in thickness, and 25.5 cm in height, and was filled with a mixture of epoxy resin and quartz sand of 80–200 mesh. The appearance and physical properties of the consolidated sandstone model are quite similar to that of natural sandstone (density is 2.82 g/cm³, and porosity is 34.12%). Two layers with different permeability were designed for the model to simulate a positive rhythm reservoir in which the permeability increased from the top to the bottom. The permeability of the upper half of the model is 1,000 md, while that of the lower half is 1,500 md. A 2-cm-thick layer of epoxy resin was cast around the artificial model to reinforce it and establish the surrounding impermeable conditions.

Before the laboratory experiment, the model was subjected to vacuum for 24 hours and then oil was imbibed to calculate porosity of the model. Water was pumped into the model at the flow rate of 5 ml/min until water content of production reached 98%, which simulated secondary development by water flooding. Gaseous CO₂ was injected into the model under an injection pressure of 50 kPa until no obvious change in production could be observed, to simulate immiscible gas flooding after water flooding.

Figure 1 Cumulative production by water and gas flooding (see online version for colours)**Figure 2** Fluid distribution of experimental model, (a) water saturation distribution after water flooding (b) CT value distribution after gas flooding (see online version for colours)

(a)



(b)

After water flooding, more than 60% of the oil was produced; in other words, considerable oil was still left in the model (Figure 1). Computerised tomography (CT) images show that most of the residual oil was located in the upper part of the model, as a result of the effects of gravity

[Figure 2(a)]. At the end of water flooding, cumulative oil production tended to be constant, but it began increasing again when gas injection started. At first, both oil and water were produced rapidly. After a period of gas flooding, no further water was pumped from the model, while oil production continued, which was different from conditions under water flooding (Figure 1). CT images indicated that at the end of gas flooding, the upper part of the model has been swept completely and the remaining oil in the model had been effectively displaced by gaseous CO₂ [Figure 2(b)]. Oil recovery increased by 22.07% through immiscible CO₂ flooding, which means immiscible displacement was efficient for enhancing oil recovery after water flooding, even in reservoirs with positive rhythm.

3 Numerical simulation setting and historical matching

As a result of the pressure resistance of the model and limits of experimental safety, the injection pressure could not be very high. Therefore, numerical simulation based on the experiment was necessary for further studies of gas displacement as an EOR method.

The numerical simulation was obtained by the CMG GEM module (Computer Modelling Group Ltd.). This module is designed for compositional models, which are used for gas and polymer flooding. In this model, reservoir fluid is divided into three phases (oil, aqueous, and gaseous) and several components. The flow process for reservoir fluid satisfies the following continuity equation:

$$\begin{aligned} & -\nabla \cdot \left[\alpha \left(C_{io} \rho_o \vec{V}_o + C_{ig} \rho_g \vec{V}_g + C_{iw} \rho_w \vec{V}_w \right) \right] + \alpha q_i \\ & = \alpha \frac{\partial}{\partial t} \left[\phi \left(C_{io} \rho_o S_o + C_{ig} \rho_g S_g + C_{iw} \rho_w S_w \right) \right] \end{aligned} \quad (1)$$

The flow also obeys Darcy's law:

$$\begin{cases} \vec{V}_o = -\frac{kk_{ro}}{\mu_o} (\nabla P_o - \rho_o g \nabla D) \\ \vec{V}_g = -\frac{kk_{rg}}{\mu_g} (\nabla P_g - \rho_g g \nabla D) \\ \vec{V}_w = -\frac{kk_{rw}}{\mu_w} (\nabla P_w - \rho_w g \nabla D) \end{cases} \quad (2)$$

On the basis of equations (1) and (2), the continuity equation can be simply expressed as:

$$\begin{aligned} & \nabla \cdot \left[\sum_j \frac{KK_{rj} \rho_j}{\mu_j} C_{ij} (\nabla P_j) - \rho_j g \nabla D \right] + q_i \\ & = \sum_j \frac{\partial}{\partial t} (\phi \rho_j S_j C_{ij}), \quad i = 1, 2, \dots, N; j = o, g, w \end{aligned} \quad (3)$$

The mass fraction and saturation also satisfy the following equations:

$$\sum_{i=1}^N C_{ij} = 1 \quad (4)$$

$$S_o + S_g + S_w = 1 \quad (5)$$

The equilibrium constant of each component, which is used to calculate the compositions of the liquid and gaseous phases, is given by the phase equilibrium equation:

$$\begin{cases} \frac{C_{ig}}{C_{io}} = K_{igo}(T, P_o, P_g, C_{io}, C_{ig}) \\ \frac{C_{ig}}{C_{iw}} = K_{igw}(T, P_o, P_w, C_{iw}, C_{ig}) \end{cases} \quad (6)$$

The density and viscosity of each phase are also related to the mass fraction of the component and phase pressure as follows:

$$\begin{cases} \rho_o = \rho_o(p_o, C_{1o}, C_{2o}, \dots, C_{No}) \\ \rho_g = \rho_g(p_g, C_{1g}, C_{2g}, \dots, C_{Ng}) \\ \rho_w = \rho_w(p_w, C_{1w}, C_{2w}, \dots, C_{Nw}) \end{cases} \quad (7)$$

$$\begin{cases} \mu_o = \mu_o(p_o, C_{1o}, C_{2o}, \dots, C_{No}) \\ \mu_g = \mu_g(p_g, C_{1g}, C_{2g}, \dots, C_{Ng}) \\ \mu_w = \mu_w(p_w, C_{1w}, C_{2w}, \dots, C_{Nw}) \end{cases} \quad (8)$$

The phase pressure and relative permeability of each phase relates to the saturation of each phase as follows:

$$\begin{cases} k_{ro} = k_{ro}(S_o, S_g, S_w) \\ k_{rg} = k_{rg}(S_o, S_g, S_w) \\ k_{rw} = k_{rw}(S_o, S_g, S_w) \end{cases} \quad (10)$$

The outer boundary conditions of the simulation are defined as closed, which are induced by the following equation:

$$\left. \frac{\partial P}{\partial n} \right|_{r_w} = 0 \quad (11)$$

The inner boundary conditions are well boundaries. For water and gas flooding, constant production and constant bottom hole pressure are used, respectively expressed as:

$$P(r_w, t) = C_1 \quad \text{for gas flooding} \quad (12)$$

$$r \left. \frac{\partial P(r, t)}{\partial r} \right|_{r_w} = C_2 \quad \text{for water flooding} \quad (13)$$

The initial conditions include reservoir pressure and distribution of fluid saturations, which are given directly.

The properties of the simulation model were identical to the experimental model, including size, porosity, and permeability. Because the experiment was a rectangular prism, a Cartesian regular grid was generated for the simulation model. Numbers for the grid in three directions (i, j, k ; for length, thickness, and height, respectively) were 10, 1, and 51. The simulated injection and production wells were set in the first and last grid of the i direction and fully penetrated. The main setting parameters for the simulation model are given in Table 1.

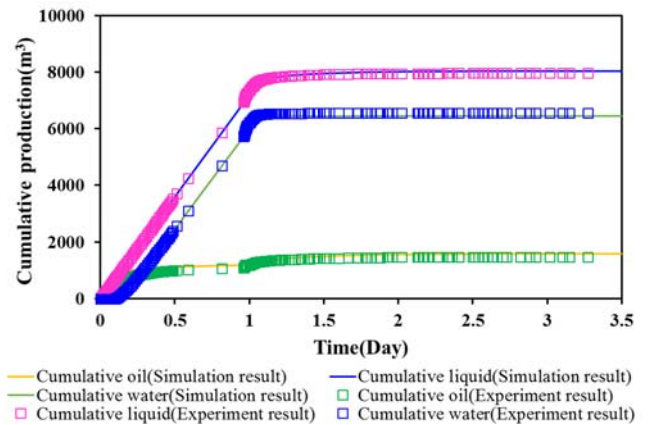
Cumulative oil and water production was imported as historical production data of the simulation model, to optimise the physical properties and make fluid migration close to that of the experimental model.

After historical matching, the predicted cumulative liquid, oil, and water production of the simulation model were basically consistent with the laboratory experimental result (Figure 3). The simulation model was suitable for predicting gas displacement under different conditions. All of the gas injection simulations restarted from the last time node of water flooding, to ensure that all predictions were established on the same initial conditions.

Table 1 Main setting parameters of the simulation model

Grid numbers (i, j, k)	10, 1, 51
Grid size (i, j, k)	0.05 m, 0.04 m, 0.005 m
Permeability	1,000 md (rows 1–25 along k direction) 1,500 md (rows 26–51 along k direction)
Total porosity	34.12%
Producer location	10, 1, 1
Injector location	1, 1, 1
Injector constraints	Water flooding: maximum surface water rate: 0.0072 m ³ /day Gas flooding: Maximum bottom hole pressure: injection pressure
Producer constraints	Minimum bottom hole pressure: 115.325 kPa
Initial pressure	115.325 kPa
Initial saturation	Oil: 1, water: 0, gas: 0
Simulated production time	Water flooding: 0.96313 days Gas flooding: 4.14857 days

Figure 3 Historical matching results for the simulation model (see online version for colours)



4 Effect of injection pressure

Several injection-production pressure differences, between 10 kPa and 1,000 kPa, were chosen for simulation. The trends of oil production were all similar under different

injection pressures: the early stage of gas flooding was the period of rapid oil accumulation [Figure 4(a)]. However, final oil production and increases in oil recovery were dissimilar for different injection pressures. With increasing injection pressures, increased oil recovery grew rapidly and reached a maximum; and then began to decrease to a very

low rate [Figure 4(b)]. Considering the extra costs of increasing pressure, an optimal injection pressure could be determined according to actual conditions. For this simulation model, the maximum increased oil recovery appeared at the injection-production pressure difference of 150 kPa, but optimal values should be further investigated.

Figure 4 The relationship between effects of enhanced oil production by gas flooding and injection-production pressure differences, (a) cumulative oil production under various pressure differences (b) increased oil recovery under various pressure differences (see online version for colours)

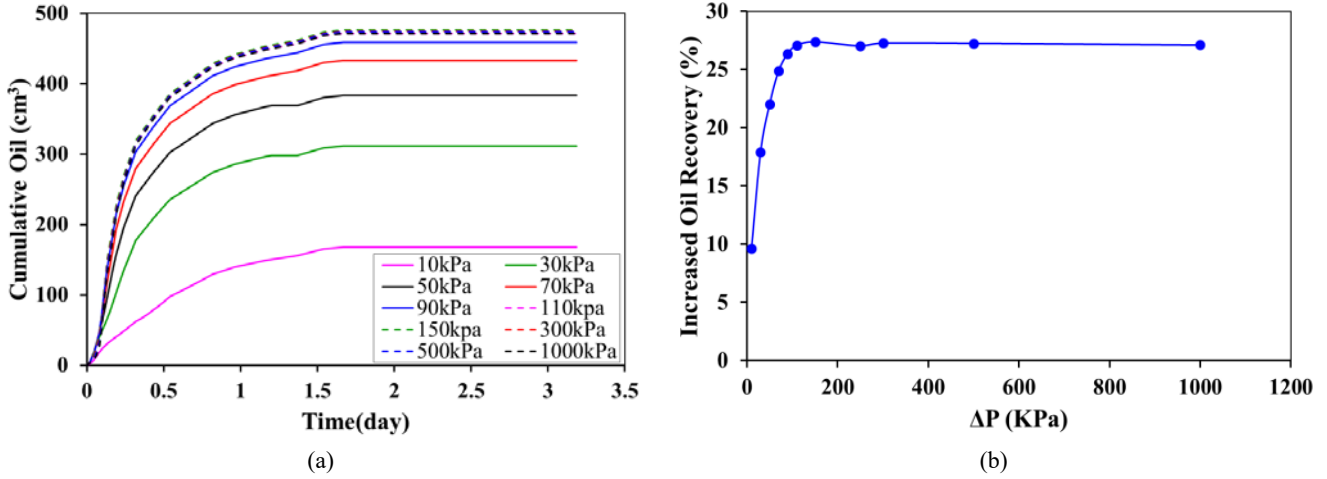


Figure 5 Relationship between effects of enhanced oil production by gas flooding and confining pressure, (a) cumulative oil production under different confining pressures, $\Delta P = 10$ kPa (b) cumulative oil production under different confining pressures, $\Delta P = 50$ kPa (c) cumulative oil production under different confining pressures, $\Delta P = 150$ kPa (d) the change in increased oil recovery under different confining pressures (see online version for colours)

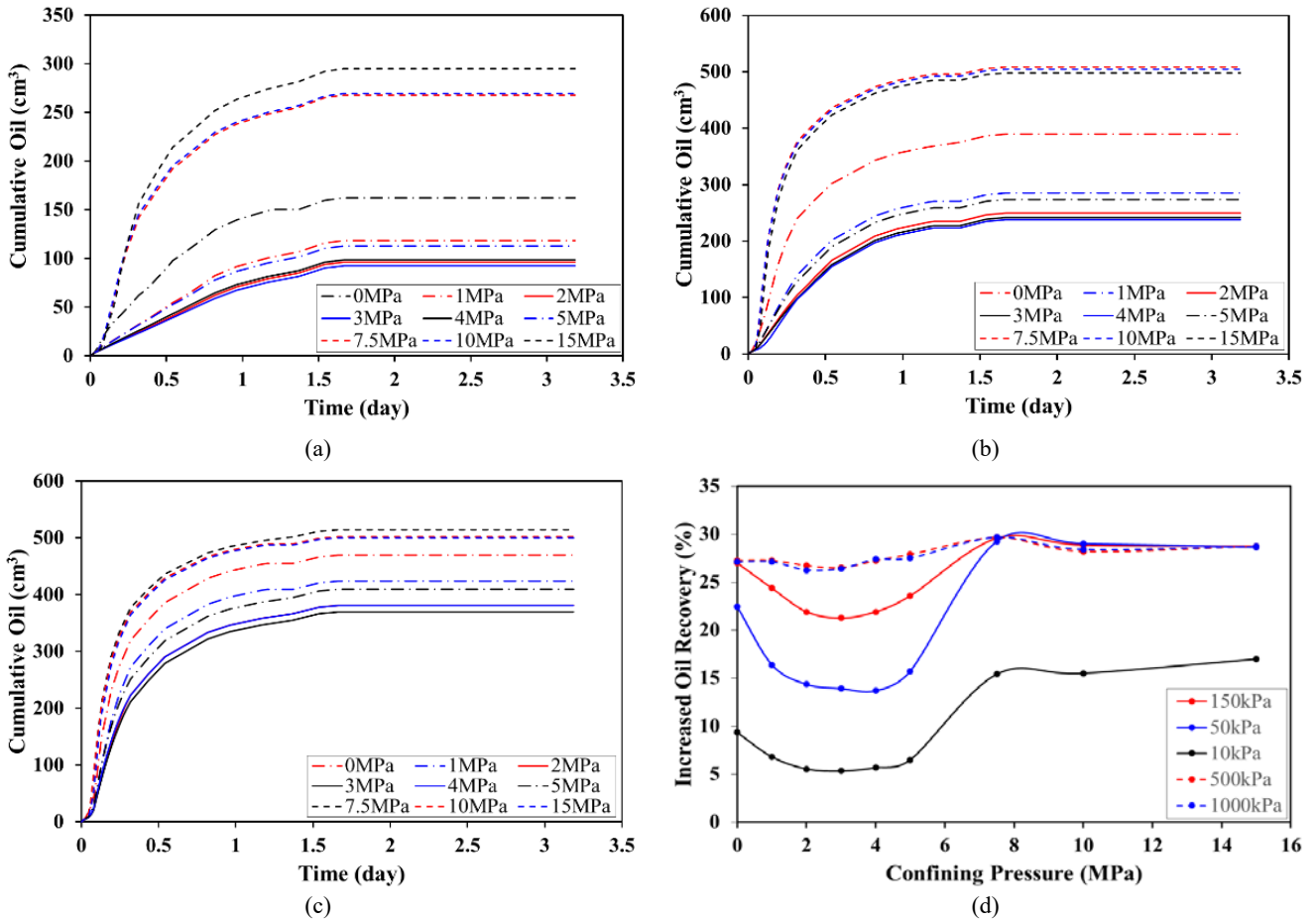
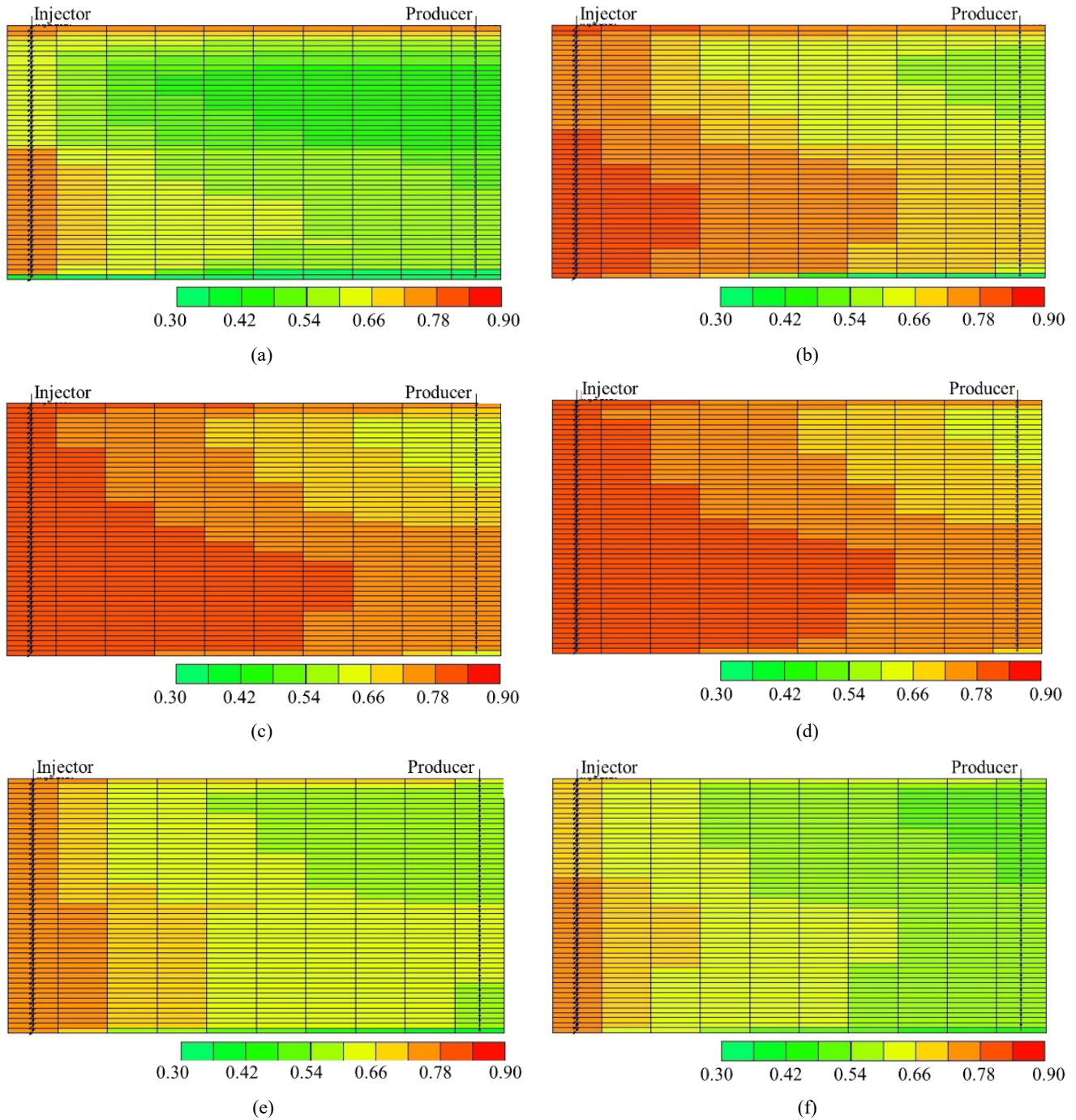


Figure 6 Gas saturation of CO₂ after miscible gas flooding (a) $\Delta P = 10$ kPa, without confining pressure (b) $\Delta P = 50$ kPa, without confining pressure (c) $\Delta P = 150$ kPa, without confining pressure (d) $\Delta P = 500$ kPa, without confining pressure (e) $\Delta P = 50$ kPa, confining pressure = 1 MPa (f) $\Delta P = 50$ kPa, confining pressure = 3 MPa (see online version for colours)



5 Effect of confining pressure

Because metal causes artefacts in CT images, it was difficult to provide either a special clamping device or extra confining pressure for such a large experimental model. Therefore, the simulation was also used to research the effect of confining pressure on increased oil recovery by gas flooding. Several confining pressures between 1 MPa and 15 MPa were tested on the simulation model. With increasing confining pressure, increased oil recovery by gas flooding decreased at first. When confining pressure was

higher than 5 MPa, increased oil recovery by gas flooding began to increase, and then tended to be almost constant (Figure 5). It can be inferred that increased oil recovery was a result of the occurrence of miscible displacement. Therefore, optimal oil recovery by gas flooding was also affected by confining pressure. When the injection-production pressure difference was much lower than the confining pressure, oil recovery increased dramatically, although the change was not very obvious when the two were well matched. Consequently, reservoir pressure

conditions should be considered carefully when choosing the injection pressure for immiscible gas displacement.

6 Migration of gaseous CO₂ during gas flooding

Although the permeability of the lower part of the model is higher than that of the upper part, during gas flooding the gaseous CO₂ established new flow channels in the upper layers of the model first, instead of causing breakthrough in the high permeability layers in the lower part of the model. Areas with high gas saturation even appeared on the surface of the model [Figures 6(a) to 6(d)]. This was mainly because of the effect of gravity. Under low injection pressures, lack of driving force restricted the migration of CO₂; therefore, the sweep volume of CO₂ was very limited in both the high-permeability layer and the low-permeability layer [Figures 6(a) and 6(b)]. With increasing injection pressures, more space was occupied by gas. When the injection pressure was higher than the optimal value the driving force mainly dominated the flow of CO₂ resulting in quick breakthrough in the high-permeability layers, although CO₂ still swept the low permeability layers which [Figures 6(c) and 6(d)]. Hence, oil recovery did not change too much further. Sweep efficiency decreased again under confining pressure [Figures 6(e) and 6(f)], because of resistance increasing in pores and the decline of gravity effects caused by CO₂ compression. This could partly explain the relationship between injection pressure and increased oil recovery by immiscible CO₂ flooding.

7 Conclusions

A numerical simulation model was established based on a laboratory experiment to study immiscible CO₂ flooding as a tertiary oil recovery method. Predictions from numerical simulations indicated that immiscible CO₂ flooding was an effective EOR method for thick reservoirs after water flooding. Through immiscible CO₂ flooding oil recovery increased significantly.

Immiscible CO₂ flooding is influenced by injection pressure and confining pressure. For certain reservoir conditions, there is an optimal injection pressure for maximum oil recovery. With increasing confining pressures, oil recovery decreased until miscible displacement occurred.

During immiscible gas flooding, the gravity effect promotes gas migration into the upper layers, which improves sweep efficiency. Increasing injection pressure may further increase CO₂ sweep volume, but excessive injection pressure may cause quick breakthrough. Confining pressure is a negative factor for CO₂ flooding. Although many efforts have been made to investigate CO₂ flooding after water flooding, it is necessary to conduct further theoretical investigations.

Acknowledgements

This work has been supported by a grant from the National Natural Science Foundation of China, No. 41602163. The first author also wishes to thank the State Key Laboratory of Enhanced Oil Recovery, Research Institute of Petroleum Exploration and Development, PetroChina, for assistance with the laboratory experiment.

References

- Al-Hinai, S.M., Al-Shureqi, H. and Van Wunnik, J.N.M. (2010) 'Steam flooding a thick heavy oil reservoir: development of numerical tools for reservoir management', *SPE*, p.SPE-129173-MS.
- Bikkina, P., Wan, J.M., Kim, Y.M., Kneafsey, T.J. and Tokunaga, T.K. (2016) 'Influence of wettability and permeability heterogeneity on miscible CO₂ flooding efficiency', *Fuel*, Vol. 166, pp.219–226.
- Cao, M. and Gu, Y.G. (2012) 'Physicochemical characterization of produced oils and gases in immiscible and miscible CO₂ flooding processes', *Energy & Fuels*, Vol. 27, No. 1, pp.440–453.
- Cao, M. and Gu, Y.G. (2013) 'Oil recovery mechanisms and asphaltene precipitation phenomenon in immiscible and miscible CO₂ flooding processes', *Fuel*, Vol. 109, pp.157–166.
- Cui, C.Z., Zhu, G.L., Liu, H.Q., Wang, Y.Z. and Zhao, X.Y. (2010) 'Energy supplement mode optimization for horizontal well development in thick positive rhythm oil reservoir', *Petroleum Drilling Techniques*, Vol. 38, No. 6, pp.88–91.
- Ding, Z.P., Tian, J., Qu, Y.G. and Luo, Y.Y. (2013) 'Developing methods optimization of giant thick buried hill reservoirs developing with stereo horizontal well pattern', *Well Testing*, Vol. 22, No. 5, pp.35–37.
- Duan, X.G., Hou, J.R., Zhao, F.L., Ma, Y.F. and Zhang, Z. (2016) 'Determination and controlling of gas channel in CO₂ immiscible flooding', *Journal of the Energy Institute*, Vol. 89, No. 1, pp.12–20.
- Gu, J.W. and Zhai, S.K. (2005) 'Influence factors reservoir for tapping positive rhythm thick oil potential with horizontal wells', *Journal of the University of Petroleum*, Vol. 29, No. 2, pp.61–64, China.
- Liu, F.L., Guthrie, C.F. and Shipley, D. (2012) 'Optimizing water injection rates for a water-flooding field', *SPE*, p.SPE-157996-MS.
- Liu, Y. (2012) 'Research on increasing oil well productivity of thick reservoir by water flooding and nature gas injection', *Drilling & Production Technology*, Vol. 35, No. 2, pp.48–50.
- Niu, J.F., Wang, X.Z., Wang, X.H., Gong, W.P. and Hou, H. (2006) 'Methodical study on remaining oil in thick reservoir at extra high water cut stage', *Journal of Oil and Gas Technology*, Vol. 28, No. 4, pp.345–347.
- Qu, Z.Q., Li, Y., Lin, S.S., Jiang, H.Y., Wang, P. and Huang, D.S. (2014) 'Parameter optimization of well pattern for heavy oil reservoir with thick layer exploited by THAI technology', *Fault-Block Oil & Gas Field*, Vol. 21, No. 5, pp.627–631.
- Ren, B., Zhang, L., Huang, H.D., Ren, S.R., Chen, G.L. and Zhang, H. (2015) 'Performance evaluation and mechanisms study of near-miscible CO₂ flooding in a tight oil reservoir of Jilin oilfield China', *Journal of Natural Gas Science and Engineering*, Vol. 27, No. 3, pp.1796–1805.

- Romero-Zerón, L. (2012) *Introduction to Enhanced Oil Recovery (EOR) Processes and Bioremediation of Oil-contaminated Sites*, InTch Press, Rijeka, Croatia.
- Song, Y.C., Zhu, N.J., Zhao, Y.C., Liu, Y., Jiang, L.L. and Wang, T.L. (2013) 'Magnetic resonance imaging study on near miscible supercritical CO₂ flooding in porous media', *Physics of Fluids*, Vol. 25, No. 5, p.053301.
- Sun, Y.K., Li, Q., Yang, D.X. and Liu, X.H. (2016) 'Laboratory core flooding experimental systems for CO₂ geosequestration: an updated review over the past decade', *Journal of Rock Mechanics and Geotechnical Engineering*, Vol. 8, No. 1, pp.113–126.
- Tan, G.M. (2009) 'Study on exploiting the remaining oil of thick pay zone with positive rhythm by horizontal wells', *Offshore Oil*, Vol. 29, No. 2, pp.73–77.
- Wang, B., Wang, X., Liu, X.B. and Li, S.L. (2006) 'Technique of controlling water cut and increasing oil production by injecting nitrogen foam in thick reservoirs in later high water cut stage', *Petroleum Geology & Oil Field Development in Daqing*, Vol. 25, No. 2, pp.59–60.
- Wang, M.C., Zhu, W.Y. and Shi, C.F. (2012) 'Numerical simulation study on remaining oil distribution for L thick reservoir', *Fourth International Conference on Computational and Information Sciences*, pp.147–150.
- Wang, T.L., Song, Y.C. and Zhao, Y.C. (2013) 'Measurement of immiscible CO₂ flooding processes and permeability reduction due to asphaltene precipitation by X-ray CT imaging', *Energy Procedia*, Vol. 37, Nos. 3–4, pp.6920–6927.
- Wen, H. (2012) *A Study on Remaining Oil Distribution of Heterogeneous Thick Oil Reservoirs in High-water-cut Stage*, PhD thesis, Yangtze University, Wuhan, PR China.

Glossary

C	Mass fraction of component
S	Fluid saturation
ρ	Fluid density
μ	Fluid viscosity
K_r	Relative permeability
\varnothing	Porosity
P	Pressure
\vec{v}	Mass velocity
q	Injection rate
o, g, w	Oil phase, aqueous phase and gaseous phase
